Available online at www.sciencedirect.com
SCIENCE DIRECT
Biosensors and Bioelectronics 21 (2006) 1859–1866
BIOSENSORS & BIOELECTRONICS
www.elsevier.com/locate/bios

Labeling tumor cells with fluorescent nanocrystal–aptamer bioconjugates

Ted C. Chu [a,1], Felice Shieh [b,1], Laura A. Lavery [a], Matthew Levy [a], Rebecca Richards-Kortum [c], Brian A. Korgel [b,*], Andrew D. Ellington [a,*]

[a] *Institute for Cellular and Molecular Biology, University of Texas at Austin, Austin, TX 78712, United States*
[b] *Department of Chemical Engineering, Center for Nano- and Molecular Science and Technology, Texas Materials Institute, University of Texas at Austin, Austin, TX 78712, United States*
[c] *Department of Bioengineering, Rice University, Houston, TX 77251-1892, United States*

Received 19 September 2005; received in revised form 6 December 2005; accepted 6 December 2005
Available online 21 February 2006

Abstract

Aptamers that bind to prostate specific membrane antigen (PSMA) were conjugated to luminescent CdSe and CdTe nanocrystals for cell-labeling studies. The aptamer–nanocrystal conjugates showed specific targeting of both fixed and live cells that overexpressed PSMA. More importantly, aptamers were able to label cells dispersed in a collagen gel matrix simulating tissue. The specific binding abilities and synthetic accessibility of aptamers combined with the photostability and small size of semiconductor nanocrystals offers a powerful and general tool for cellular imaging.

Keywords: Nanocrystal; Aptamer; Cell imaging

1. Introduction

Prostate cancer affects approximately 1 in 11 men and it is the second leading cause of cancer deaths among American males (Greenlee et al., 2001). As with all cancers, early detection offers the best prospects for patient survival. Prostate cancer screening currently relies on rectal examinations to detect anomalies in the prostate gland, along with blood tests for upregulated prostate specific antigen (PSA) levels (Nelson, 2002). However, rectal examinations are invasive, and blood tests can sometimes be inconclusive, as PSA levels in the blood may be heightened by factors other than carcinoma (Untergasser et al., 2005). Taken as a whole, these diagnostic methods are prone to significant false-positive rates and exhibit relatively poor sensitivity (Postma and Schroder, 2005). In contrast to PSA, prostate specific membrane antigen (PSMA), a membrane-bound glycoprotein, is overexpressed in many prostate cancers (Nelson, 2002). More specifically, high levels of PSMA have been found in patients with hormone-insensitive prostate cancer cells (Bostwick et al., 1998; Kawakami and Nakayama, 1997) as well as in the neovasculature associated with other solid malignant tumors (Liu et al., 1997). This well-characterized, integral membrane protein has therefore been identified as a good indicator of cancer growth and metastases. In fact, a variety of anti-PSMA-based therapies are currently under investigation (Chang, 2004; Slovin, 2005; Tricoli et al., 2004).

One approach to PSMA detection has been to target fluorescent markers to tumors via monoclonal antibodies (Barren et al., 1998; Liu et al., 2002). While nanocrystal–antibody conjugates against PSMA have previously been used to image cancer cells implanted in live mice (Gao et al., 2004), the large size and immunogenicity of antibodies may limit their pharmacological value. Humanized antibodies, antibody fragments, and short peptides isolated from processes such as phage display are also possible affinity reagents, but are similarly susceptible to peptidase fragmentation and immune response (Jayasena, 1999).

Selected nucleic acid binding species (aptamers) are alternative affinity reagents (reviewed in Jayasena, 1999). Aptamers have previously been selected against a variety of targets ranging from small molecules to proteins to cell surfaces. Aptamers typically bind their targets with nanomolar or better affinities and have specificities comparable to those of monoclonal antibodies (Jenison et al., 1994). Moreover, modified nucleotides can be introduced into aptamers that render them highly resistant to

* Corresponding authors. Tel.: +1 512 471 5633; fax: +1 512 471 7060.
E-mail addresses: korgel@mail.che.utexas.edu (B.A. Korgel), andy.ellington@mail.utexas.edu (A.D. Ellington).
[1] These authors contributed equally to this work.

0956-5663/$ – see front matter © 2006 Published by Elsevier B.V.
doi:10.1016/j.bios.2005.12.015

nuclease digestion (Beigelman et al., 1995). Finally, aptamers can be chemically synthesized in bulk. Taken together, these features may make aptamers an ideal choice for cancer diagnosis and therapy.

In this regard, aptamers have already been selected to bind to prostate specific membrane antigen and the fluorescently labeled anti-PSMA aptamer, A10, has been shown to specifically bind PSMA-expressing prostate tumor cells (LNCaP cells; Lupold et al., 2002). Little or no labeling was observed with a non-PSMA-expressing prostate tumor cell line (PC3 cells; Lupold et al., 2002). More recently, the same anti-PMSA aptamer has been used to localize polylactate/PEG nanoparticles to the surface of PSMA-expressing tumor cells (Farokhzad et al., 2004). Localization was associated with internalization of the nanoparticle, demonstrating a potentially novel therapeutic application for aptamer:nanoparticle conjugates.

Quantum dots offer a number of significant advantages over traditional fluorophores. Compared to organic dyes, which generally have low photostabilities, narrow excitation spectra, and broad emission bands, quantum dots have relatively good photostabilities and tunable color with narrow emission spectra (Lim et al., 2003; Michalet et al., 2005). These properties potentially make quantum dots useful reagents for multispectral in vivo diagnostic imaging of cells, tissues, and living animals. We now demonstrate the use of anti-PSMA aptamer:quantum dot conjugates for the specific labeling of PSMA-expressing prostate tumor cells both in cell culture and in simulated tissue samples using the alternate anti-PSMA aptamer A9 (Lupold et al., 2002). In all cases, binding was found to be sensitive and specific for cell lines overexpressing the PSMA antigen.

2. Methods and materials

2.1. Cell culture

LNCAP cells (ATCC CRL-1740) and PC3 cells (ATCC CRL-1435) were purchased from ATCC. LNCaP cells were incubated in RPMI 1640 (Gibco) media supplemented with 2 mM L-glutamine, 1.5 g/L glucose, 10 mM Hepes, 1.0 mM sodium pyruvate, and 10% FBS. PC3 cells were incubated in HAM's F12K media (ATCC) supplemented with 2 mM L-glutamine, 1.5 g/L sodium bicarbonate, and 10% FBS. Cells are incubated at 37 °C in 10 mL media until 90% confluence. Cells were trypsinized and subcultured at a split ratio of 1:6 to 1:10. LNCaP and PC3 cells were used between passage 4 and 40 for experiments with approximately 1 million cells adhered as a monolayer to a 0.5 mm depth coverwell (Fisher Scientific).

2.2. Aptamer synthesis and preparation of QD525 conjugates

The selection and characterization of anti-PSMA aptamers has previously been described (Lupold et al., 2002). All RNAs were synthesized by runoff transcription from double stranded DNA templates bearing a T7 promoter. All transcriptions contained 2′F-UTP and 2′F-CTP. For conjugation to quantum dots, the anti-PSMA aptamers were oxidized at the 3′ end using sodium periodate followed by reaction with biotin hydrazide (Qin and Pyle, 1999). Biotinylated anti-PSMA aptamer was complexed with Quantum dot 525 streptavidin conjugates (Quantum Dot Corporation, CA), followed by blocking with excess free biotin. As a control, a RNA pool that contained 30 random sequence positions (N30; ((Lato et al., 1995)) was also biotinylated and used to label quantum dots.

2.3. Determination of the apparent dissociation constant for anti-PSMA aptamer A9

Increasing concentrations of aptamer A9 were incubated with 3×10^5 LNCAP cells for 30 min in PBS. The cells were pelleted and washed three times with PBS. The bound aptamer was recovered from labeled cells by adding 300 μl trizol to lyse the cells followed by addition of 300 μl of 25:24:1 phenol:chloroform:isoamyl alcohol, followed by with ethanol precipitation and suspended in 30 μl of water. Collected aptamers were used for reverse-transcription PCR. Two primer sequences were applied (TTCTAATACGACTCACTATAGGGAGGACGATGCGG, TCGGGCGAGTCGTCTG), followed by heating at 70 °C for 30 min and then cooling to room temperature prior to the addition of taq polymerase and reverse transcriptase. Reverse-transcription was performed at 50 °C for 10 min followed by 12 PCR cycles at 94 °C for 15 s, 45 °C for 15 s, 72 °C for 30 s, and 72 °C for 2 min. PCR products were analyzed on a native 8% polyacrylamide gel. The gels were stained with SybrGold and the intensity of the bands corresponding to full length product determined using a Molecular Imager FX Pro Plus MultiImager System, and Quantity One 1-D Analysis Software (Bio-Rad, Hercules, CA).

2.4. Aptamer:QD525 conjugate cell labeling

Cells were grown to 80% confluence in a T25 flask followed by trypsin treatment 37 °C for 5 min. Cells were then washed with media plus 10% FBS to neutralize the trypsin and three times with PBS. 3×10^5 cells were used for each test. Cells were then fixed with 4% formaldehyde plus 0.01% sodium azide in PBS followed by wash in PBS three times 5 min each. About 80 μg/ml BSA in PBS was added to block the cell surface. Three microliters of biotinylated anti-PSMA aptamer:QD525 streptavidin complex was added to a 5 nM final concentration, which was incubated on ice for 60 min. Unbound aptamer was removed by washing three times with PBS. DAPI nucleic stain was performed by adding DAPI to 1 μg/ml final concentration at room temperature for 10 min followed by washing three times with PBS. Cells were then mounted with 30% glycerol in PBS.

Images were taken using a Zeiss (Germany) Axioplan2 microscope with filters for FITC (excitation BP450-490, emission BP515-565), DAPI (excitation D360/40, emission D460/50).

2.5. CdTe nanocrystal synthesis

CdTe nanocrystals were made using standard airless procedures on a Schlenk line under nitrogen. In a three-neck flask

on a Schlenk line, 0.11 g CdO (0.88 mmol, 99.5%, ~1 μm powder, Aldrich) and 0.43 g tetradecylphosphonic acid (TDPA) (~1.5 mmol, 97%, Alfa Aesar) were added to 7 g trioctylphosphine oxide (TOPO) (~180 mmol, 99%, Aldrich) and purged with nitrogen for 2 h at 65 °C. In a separate flask, 0.13 g tellurium powder (~1 mmol, 99.8%, Aldrich) was dissolved in 5 mL of trioctylphosphine (TOP, ~20 mmol, technical grade 90%, Fluka) at 120 °C under nitrogen. The CdO:TDPA:TOPO mixture was then heated to 340 °C to ensure Cd–TDPA complexation. The Cd–TDPA complex forms at temperatures as low as 290 °C, however, the most crystalline, luminescent, and size-monodisperse nanocrystals form when the CdO:TDPA:TOPO mixture is first heated to 340 °C and then cooled to the desired Te precursor injection temperature. The CdO precursor mixture was cooled to 300 °C and the tellurium precursor solution was rapidly injected under rapid stirring. Immediately following injection of the tellurium precursor, the reaction flask was removed from the heating mantle and allowed to cool. At 65 °C, 5 mL of chloroform is injected into the reaction flask to help prevent further nanocrystal growth.

2.6. CdTe nanocrystal ligand exchange, PEGylation and aptamer conjugation

The hydrophobic capping ligands, TDPA, TOP and TOPO, were exchanged with mercaptopropionic acid (MPA) under nitrogen in the reaction flask immediately after cooling the crude nanocrystal preparation to room temperature without purification. After adding the 5 mL of chloroform to quench the reaction, 10–20 mL of 0.5 M MPA (Fluka) in methanol with a 20 mol% excess of KOH, relative to the MPA mole concentration, to achieve a final concentration of approximately 1:40 mole excess of MPA to cadmium molecules (Wuister et al., 2003). The mixture was stirred overnight under nitrogen at 60 °C. The nanocrystals were then isolated as a precipitate by centrifugation at 7500 rpm for 10 min at 15 °C. The nanocrystals were further purified by redispersion in 5 mL deionized water, followed by the addition of 20 mL isopropyl alcohol as an anti-solvent to form a turbid solution. The dispersion was stored for 4 h at 4 °C, and then centrifuged at 7500 rpm for 10 min at 15 °C to isolate the nanocrystals. Precipitated nanocrystals readily dispersed in water, indicating successful ligand exchange. For storage, the MPA-capped nanocrystals were redispersed in deionized water and aliquoted into 1 mL vials and lyophilized. The nanocrystals were stored under nitrogen until needed.

MPA-capped CdTe nanocrystals were PEGylated using a single-step partial ligand exchange with equimolar concentrations of thiolated-polyethylene glycol (HS-PEG, MW 2000) and biotinylated–thiolated polyethylene glycol (HS-PEG-biotin, MW 3400) (Nektar therapeutics). Lyophilized MPA-capped CdTe nanocrystals were resuspended in 1× PBS (phosphate buffered saline, Aldrich) using the following nanocrystal concentrations on a Cd atomic basis: 30 nM CdTe nanocrystals for monolayer cell labeling and 300 nM CdTe nanocrystals for tissue phantom labeling. SH-PEG-biotin and SH-PEG in 1× PBS were added to the nanocrystal dispersions to a final concentration of 10 μM for monolayer cell labeling and 100 μM for tissue phantom labeling. The PEG/nanocrystal solutions were rocked for 1 h at room temperature.

Biotinylated PEGylated-CdTe nanoparticles were conjugated to anti-PSMA aptamer using avidin linking. Avidin (Avidin/Biotin blocking kit, Vector Laboratories) was added in large excess to the nanocrystals to minimize cross-linking between particles. For monolayer cell labeling, avidin was added to a final concentration of 20 μM to the nanocrystal/PEG solutions (for a PEG-biotin:avidin mole ratio of 1:2) and rocked at room temperature for 15 min. Two microliters of 85 nM biotinylated-aptamer was then added to the nanocrystal dispersion and rocked for 30 min at room temperature. Excess biotin was added to block remaining avidin sites (19.2 μL for cell monolayer labeling) to a final concentration of 128 μM and incubated for 15 min with rocking at room temperature. No evidence of particle cross-linking was observed under these conditions. For tissue phantom labeling, final avidin, biotin, and aptamer concentrations were 200 μM, 1.28 mM, and 800 nM, respectively.

2.7. Aptamer:CdTe conjugate cell labeling

LNCaP and PC3 cells were seeded on poly-L-lysine coated glass cover slides in 0.5 mm depth wells. Cells were cultured according to standard ATCC protocols in RPMI 1640 media (Gibco). Cells were collected from 90% confluent cell culture plates by aspirating off the media and incubating with 2 mL trypsin for 2 min at 37 °C. Two micoliters of media was added to dilute the neutralize the trypsin solution. This solution was transferred into a 50 mL centrifuge tube and centrifuged to a cell pellet at 1000 rpm for 5 min at room temperature. Cells were counted using a hemocytometer and redispersed in media to obtain 1–2 million cells per well. Cells were plated in the wells at a volume of 500 μL per well and allowed to adhere to the cover glass slip overnight as a monolayer. Prior to exposure to nanocrystals, the cells were blocked with 0.05% BSA in PBS for 1 h at room temperature and then rinsed once with 1× PBS.

The cells were incubated with the aptamer:nanocrystal conjugates for 1 h at room temperature with rocking. Cells were then washed three times with 1× PBS to remove unbound nanocrystals. Cover wells were prepared for imaging on the deconvolution microscope by filling the well with 500 μL of PBS to sustain cell viability and covering the well with a 40 mm glass cover slip. To affirm that exposure to nanoparticle–aptamer bioconjugates did not affect cell viability, viability was tested before and after exposure to CdTe–aptamer conjugates with trypan blue in dilute PBS. An entire cell stained blue indicated that cells were dead; whereas blue staining solely around the perimeter of the cells, as observed during the counting of cells, was indicative of cell viability. Trypan blue staining of cells indicated that the cells remained viable after exposure and labeling with quantum dot aptamer conjugates. Deconvolution microscopy was performed on a Zeiss KS-400 using a TRITC excitation filter with an excitation wavelength of 543 nm and a long bandpass emission filter of 590 nm.

2.8. Tissue phantom (collagen-cell matrix) preparation

LNCaP or PC3 cells were collected from four to six confluent plates. The growth media was aspirated, followed by one wash with 2 mL 1× PBS. The cells were detached from the plates by adding trypsin: PC3 and LNCaP cells were incubated for 2 min at 37 °C and room temperature, respectively. Two microliters of phenol free media (Gibco) was added before transferring the cells into a 50 mL centrifuge tube. The cell dispersions were centrifuged at 1000 rpm for 5 min at room temperature. The supernatant was discarded and the pellet was resuspended in 4–6 mL of phenol free media (1 mL/plate). Cells were then counted by staining with trypan blue (50 μL trypan blue + 50 μL PBS + 50 μL cell solution). 8×10^6 cells were suspended in 80 μL of collagen matrix solution (7 parts collagen, 1.11 parts 1× PBS, 0.89 part 10× PBS, and 1 part Hepes–NaOH solution) per well prepared cold (4 °C). After suspending the cell pellet in the collagen matrix solution, it was transferred into a transwell, which was placed in a 24 well plate. After 30 min of incubation, 500 μL of phenol free media was added underneath the transwell and topped with 100 μL of media above the matrix. The tissue phantom was incubated at 37 °C overnight prior to aptamer:nanocrystal conjugate labeling.

2.9. Tissue phantom labeling

Prior to exposure to aptamer:CdTe nanocrystal conjugates, the collagen-cell matrix, or tissue phantom, was blocked with 0.05% BSA in PBS for 1 h at room temperature. The media and BSA were aspirated and 200 μL of aptamer–quantum dot conjugates in 1× PBS at a concentration of 300 nM CdTe (on a Cd atomic basis) and 800 nM aptamer were added to the tissue phantom and incubated for 1 h at room temperature. The tissue phantom was washed three times with 1× PBS and then cut out of the transwell and prepared for slicing by suspending in 3 wt.% agarose. Tissue slices were 200 μm thick and mounted on a 60 mm coverslip for imaging with a Leica SP2, AOBS confocal microscope.

3. Results and discussion

Cell binding studies utilized the anti-PSMA aptamer A9, a 70-mer modified RNA that contained 2′-fluoropyrimidine residues to stabilize it against serum nucleases. Previous studies had used a different anti-PSMA aptamer (A10) with approximately 10-fold lower binding affinity to PSMA (Lupold et al., 2002). While A9 was known to bind tightly to PSMA, it was not known whether it could bind to cell surfaces expressing PSMA. As a prelude to labeling experiments, we used conventional molecular biology assays to confirm binding. LNCaP and PC3 prostate tumor cell lines were incubated with the aptamer, washed, and the aptamer was recovered by cell lysis with trizol. Bound aptamers were then amplified via reverse-transcription and PCR. As shown in Fig. 1, small amounts of aptamer were recovered from PC3 cells, but much more was recovered from LNCaP cells, as expected given that PSMA overexpression occurs in this cell line.

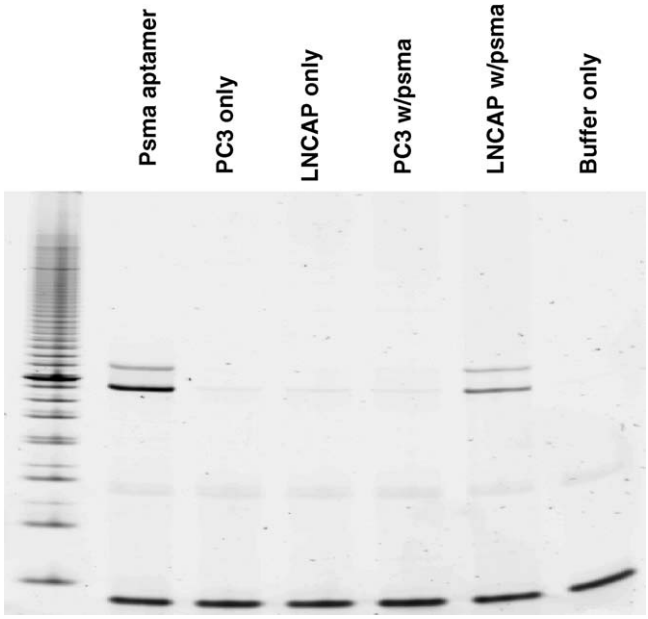

Fig. 1. RT/PCR of cell lysate from binding assay. From left to right, lane 1: 10 bp marker. Lane 2: pure PSMA aptamer. Lane 3: lysate of PC3 cells without incubated with PSMA aptamer. Lane 4: lysate of LNCAP cells without incubated with PSMA aptamer. Lane 5: lysate of PC3 cells incubated with PSMA aptamer. Lane 6: lysate of LNCAP cells incubated with PSMA aptamer. Lane 7: buffer only.

Having demonstrated specific binding to the cell surface, we then quantified the A9 binding affinity by varying the aptamer concentration from 0.1 nM to 2 μM, while keeping the number of LNCap cells constant at 3×10^5 per 50 μl. As shown in Fig. 2, the amount of RNA recovered increases linearly with concentration between 1 and 32 nM, suggesting the Kd for whole cells is ∼5-fold lower than the K_i measured for the free protein (2.1 nM; Lupold et al., 2002). At 100 nM, the binding curve levels off suggesting saturation of cell surface binding sites. Assuming 100% binding efficiency of the aptamer to the target, this corresponds to $\sim 10^6$ sites on the surface of each cell.

Given that A9 has a strong binding affinity to PSMA on the surface of LNCaP cells, we explored cell surface labeling with

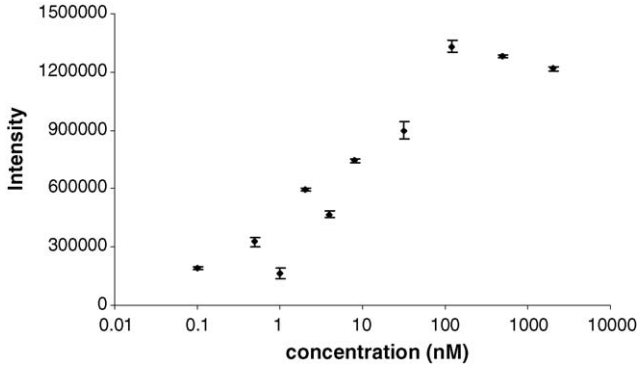

Fig. 2. PSMA aptamer binding curve. LNCAP cells were incubated with increasing concentrations of aptamer A9. After washing, the cells were treated with trizol. Recovered aptamers were reverse transcribed, amplified by 12 cycles of PCR and analyzed by gel electrophoresis. Relative binding was determined by comparing the fluorescent intensity of the PCR products on the gel.

aptamer:quantum dot conjugates. Aptamer A9 was synthesized by in vitro transcription and was biotinylated at its 3′-end by periodate oxidation and conjugation to biotin hydrazide (Qin and Pyle, 1999). The biotinylated aptamers were in turn immobilized on streptavidin-coated CdSe and CdTe nanocrystals and tested for labeling of both fixed and live cells.

Initial binding studies were conducted using commercially available CdSe nanocrystals to make aptamer:QD525 (Quantum Dot corporation) conjugates, which were then exposed to fixed cells. Biotinylated aptamers were incubated with streptavidin-coated quantum dots in a 1:1 ratio. After conjugation, the remaining biotin binding sites on the streptavidin-coated quantum dots were blocked with an excess of free biotin (Fig. 3). LNCaP and PC3 adherent cells (3×10^5 cells) were prepared for labeling by growing them to 80% confluence and then suspending them following treatment with trypsin at 37 °C for 5 min. The cell suspensions were centrifuged and the cells were washed with media plus 10% FBS (to neutralize trypsin) and three times with PBS. Cells were then fixed with 4% formaldehyde plus 0.01% sodium azide in PBS, washed with PBS 3× additional times, and then resuspended in 50 μl. To reduce non-specific nanocrystal binding, the cells were first blocked with BSA (80 μg/ml) in PBS. The biotinylated anti-PSMA aptamer:QD525 complex (3 μl; 5 nM final concentration) was added to the cells and the labeling reaction was incubated on ice for 60 min. Unbound aptamer was removed by 3× washes with PBS. In some cases, cell nuclei were also stained with DAPI (1 μg/ml final concentration). For microscopic analysis, cells were mounted on a slide with 30% glycerol in PBS.

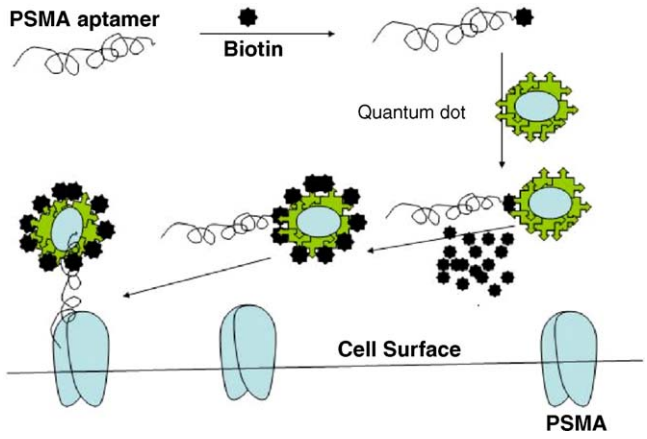

Fig. 3. Quantum dot conjugation and PSMA binding scheme.

For each labeling experiment, two sets of tissue culture cells were used: one was labeled with DAPI prior to further treatment, and one was not. Cells with blue nuclear DAPI staining could then be mixed with cells without DAPI staining to serve as a visual reference for direct comparison of labeling efficiency (Fig. 4). In the first experiment, we compared the binding of non-conjugated quantum dots with anti-PSMA aptamer:QD conjugates. LNCaP cells with nuclear DAPI staining were exposed

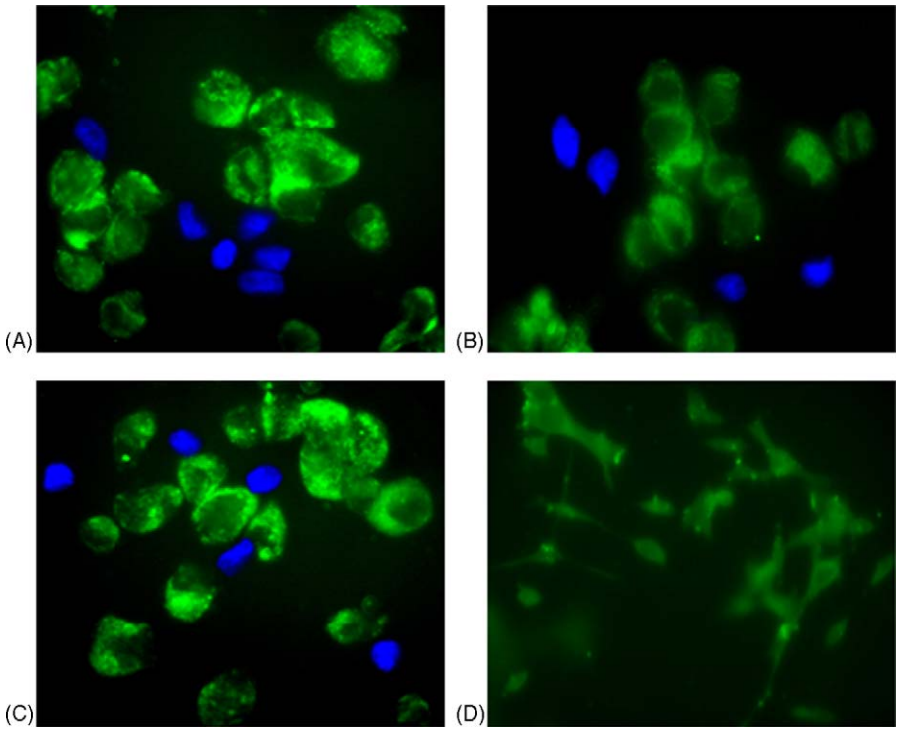

Fig. 4. Labeling of cell lines with aptamer:QD525 conjugates. (A) LNCAP cells labeled with PSMA-aptamer biotin quantum dot conjugates then mixed with LNCAP cells labeled with quantum dots only as well as nucleic staining with DAPI. (B) LNCAP cells (PSMA positive cells) labeled with PSMA-aptamer biotin quantum dot conjugates mixed with LNCAP cells labeled with random sequence aptamer as well as nucleic staining with DAPI. (C) LNCAP cells (PSMA positive cells) labeled with PSMA–aptamer biotin quantum dot conjugates mixed with PC3 cells labeled with PSMA–aptamer biotin quantum dot conjugates as well as nucleic staining with DAPI. (D) LNCAP cells in cell culture condition without suspension labeled with PSMA–aptamer biotin quantum dot conjugates.

to non-conjugated nanocrystals and LNCaP cells without DAPI staining were exposed to the aptamer:QD conjugates in separate tubes. After washing to remove any unbound label, the cells were mixed for visualization and comparison. As shown in Fig. 4A, the DAPI-stained LNCaP cells treated with the non-specific nanocrystals showed almost no signal corresponding to the quantum dot (blue nuclei, with no green halo), while LNCaP cells treated with the anti-PSMA aptamer:QD conjugate showed specific labeling (no blue nuclei, but diffuse green staining).

In the second experiment, we further evaluated binding specificity by comparing the binding of quantum dots bearing non-specific RNA molecules with the anti-PSMA aptamer:QD conjugates (Fig. 4B). Non-specific RNA QD conjugates were generated using a random sequence RNA pool as opposed to a specific aptamer. DAPI-stained LNCaP cells were incubated with the pool:QD conjugate and mixed with cells labeled with the anti-PSMA aptamer:QD conjugate for direct comparison. As shown in Fig. 4B, the DAPI-stained LNCaP cells exposed to pool:QD conjugates exhibit no observable labeling. The observed binding of the aptamer:QD conjugates appears to relate to the specific biomolecular recognition between the aptamer binding sequence A9 and PSMA, with little non-specific interaction between PSMA and the random nucleic acid sequences of the pool.

Finally, to confirm that A9 aptamer:QD conjugate labeling was directed to PSMA, PC3 cells, which do not overexpress PSMA, were exposed to the aptamer:QD conjugates to determine if labeling would occur. PC3 cells were treated with DAPI and then exposed to anti-PSMA aptamer:QD conjugates. LNCaP cells (without DAPI staining) were treated only with the conjugates (Fig. 4C). While some labeling was observed with PC3 cells (light green halo around blue), it was much less than the fluorescent labeling observed for the LNCaP cells, as expected.

All of the previous experiments were carried out with trypsinized cells to ensure uniform labeling in solution and thus avoid surface artifacts. However, when adherent, non-trypsinized LNCaP cells were labeled with anti-PSMA aptamer:QD conjugates excellent labeling was also observed (Fig. 4D), and normal adherent cell shape could easily be made out.

While CdSe nanocrystals are commercially available and serve as a good starting point for studying nanocrystal–aptamer conjugates, these nanocrystals emit too far in the blue for in vivo diagnostic applications. Tissue scatter constrains both the excitation and emission wavelengths of optical probes to the far-red and near-infrared regions of the visible spectrum, making the narrower band gap exhibited by CdTe nanocrystals better suited for in vivo imaging than CdSe (Lim et al., 2003). Therefore, we conducted additional labeling experiments with relatively bright (QY = 21%) 4 nm diameter CdTe nanocrystals emitting at 650 nm (with λ_{exc} = 550 or 543 nm).

Recent synthetic advances have led to water dispersible CdTe nanocrystals that can emit with efficiencies nearly as high as those of CdSe nanocrystals (Gaponik et al., 2002). CdTe nanocrystals were synthesized by injecting TOP:Te into a hot (320 °C) TOPO/TDPA/CdO solution (Peng and Peng, 2001). The hydrophobic ligands were exchanged with mercaptopropionic acid (MPA) to increase aqueous dispersibility and then PEGylated with a combination of thiolated polyethylene glycol (HS-PEG, MW 2000) and thiolated biotinylated PEG (HS-PEG-biotin). The HS-PEG reduced non-specific binding and HS-PEG-biotin provided docking sites for aptamer bioconjugation. Biotinylated-CdTe nanocrystals were first conjugated to avidin and which was in turn coated with the biotinylated anti-PSMA aptamer. Avidin was initially added in large excess to the nanocrystals in order to minimize cross-linking between particles prior to adding the biotinylated aptamer. Finally, excess biotin was added to block any remaining avidin binding sites on the nanocrystals.

Labeling experiments with aptamer:CdTe conjugates were carried out with live LNCaP and PC3 cells. Aptamer:QD525 conjugates were used as a positive control. PSMA-positive (LNCaP) and PSMA-negative (PC3) control cell lines were seeded onto poly-L-lysine coated glass cover slides in 0.5 mm depth wells and grown for 1 day to a monolayer consisting of approximately 1×10^6 cells per well. Cells were blocked with 0.05% BSA in PBS for 1 h at room temperature and then rinsed with PBS 1× before incubation with the nanocrystals. After exposure to nanocrystals, the cells were washed 3× with PBS and made ready for imaging on a deconvolution microscope.

As was also observed with the aptamer:QD525 conjugates, the aptamer:CdTe conjugates exhibited good labeling of live LNCaP cells. The cells exposed to PEGylated CdTe quantum dots and QD525 without aptamer conjugation exhibited almost no fluorescence (Fig. 5B and D). The negative control cell line, PC3, showed no appreciable binding to either quantum dot:aptamer conjugates or to quantum dots themselves (Fig. 5E and F). Similar to the PC3 studies, random sequence aptamer control studies were also negative, indicating selectivity of the anti-PSMA aptamer for its target (data not shown).

One long-term goal of these in vitro labeling experiments is to determine the potential for success of biomarker labeling by aptamer:nanocrystal conjugates in animal models. Towards this end, the CdTe:aptamer bioconjugates were tested for their ability to label "tissue phantoms" of LNCaP cells. Tissue phantoms are three-dimensional organotypic (RAFT) cultures of cells dispersed in a collagen gel matrix. The growth, differentiation, and morphology of cells cultured in monolayers can differ fundamentally from those cultured in three-dimensional environments (Miller et al., 1989). Cells plated on culture dishes are not supported by their normal extracellular matrix (ECM) and instead interact with the two-dimensional surface of the substrate, which causes them to flatten out (Song et al., 2000), concomitantly altering cell morphology and function (Folkman and Moscona, 1978; Gospodarowicz et al., 1978; Hoffman, 1991). In living tissue, cells also interact with each other, maintaining biochemical and mechanical functionality and homeostasis (Ingber et al., 1994; Schaper and Ito, 1996). Tissue phantoms have been shown to mimic in vivo tissues in function and growth (Gruber and Hanley, 2000; Yang et al., 1979). Tissue phantoms of both LNCaP and PC3 cell lines were studied to determine: (1) the efficacy of aptamer:CdTe nanocrystal cell labeling and (2) the extent of non-specific binding in the tissue-like network of cells.

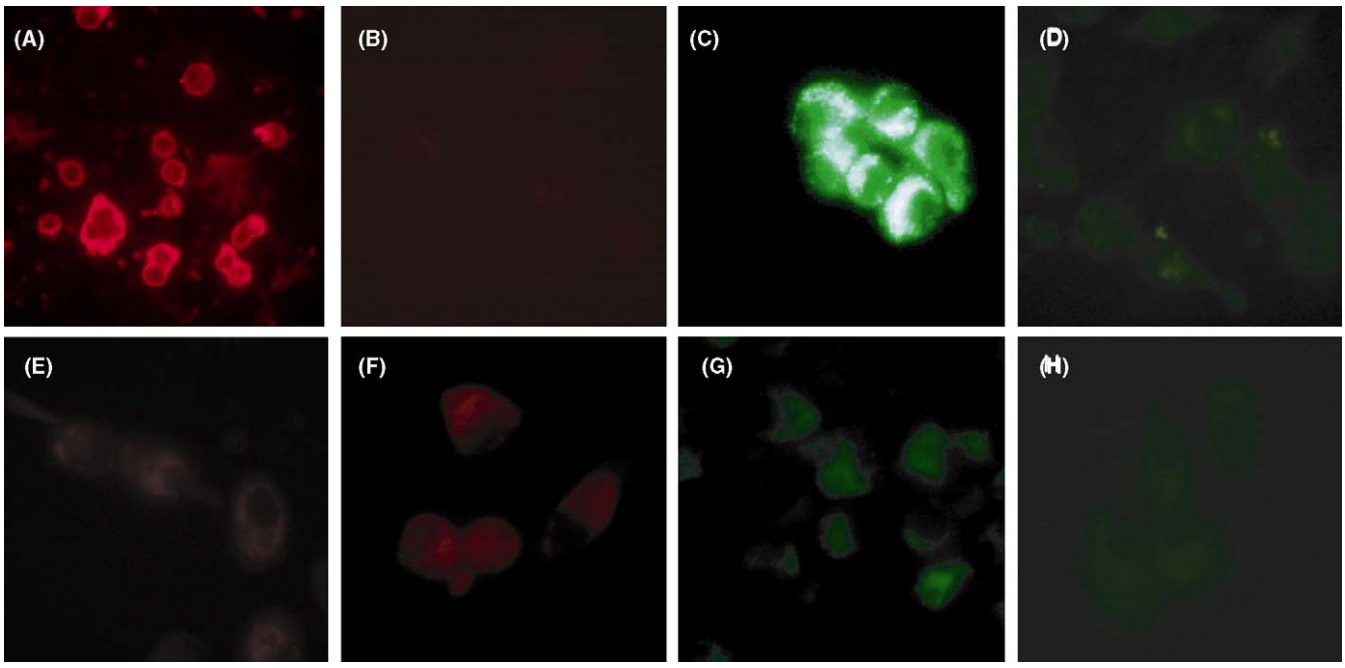

Fig. 5. Aptamer:quantum dot labeling of *live* LNCaP (A–D) and PC3 (E–H) cells: (A and E) CdTe–PSMA aptamer; (B and F) CdTe nanoparticles only; (C and G) Qdot 525–PSMA aptamer; (D and H) Qdot 525 only. Deconvolution microscopy was performed using a Zeiss KS-400 with a TRITC optical filter with an excitation wavelength of 543 nm and a long bandpass emission filter of 590 nm.

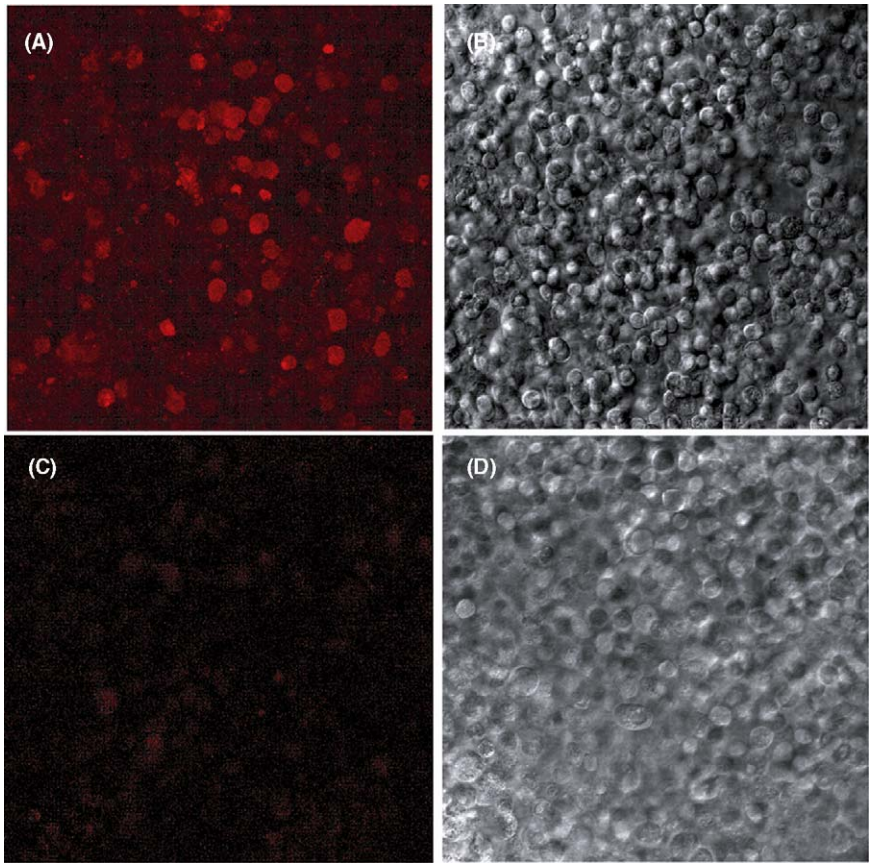

Fig. 6. LNCaP tissue phantom fluorescence (A and C) and transmitted (B and D) images labeled with (A and B) CdTe–PSMA aptamer; (C and D) CdTe quantum dots only PC3 cells showed nothing.

Fig. 6 shows fluorescence and bright-field optical microscopy images of tissue phantoms of LNCaP and PC3 cells exposed to aptamer:CdTe nanocrystal conjugates. The pictures shown in Fig. 6 are composite overlays of several images taken on a Leica SP2, AOBS confocal microscope at different focal depths in the sample. The fluorescence images were acquired using a TRITC optical filter with an excitation wavelength of 543 nm and a long bandpass emission filter of 590 nm. Cell labeling in the LNCaP tissue phantom is observed in images acquired from deep within the matrix, and prove that the nanocrystal conjugates were able to penetrate the 200 μm thick sample. Comparison of images acquired at differing depths in the tissue showed that the peripheral cells were labeled more densely than the intermediate cells. Although this could be the effect of particles being "lost to labeling" as they diffuse into the sample, it is also well-established that cells proliferate more profusely at edges of the matrix in tissue phantoms (Hoffman, 1991). The PC3 tissue phantoms exposed to aptamer:CdTe nanocrystal conjugates exhibited very little fluorescence, indicating little non-specific cell binding or capture, even in the three-dimensional cellular network. In short, the tissue phantom labeling studies confirm that aptamer:nanocrystal conjugates have the capacity to penetrate deep into tissues to label cells that present a specific biomarker.

4. Conclusions

The A9 aptamer:quantum dot conjugates exhibited specific in vitro labeling of the cell surface marker, prostate specific membrane antigen (PSMA), for fixed and live cells and live cells embedded in a collagen matrix (a tissue phantom). The specific binding abilities and synthetic accessibility of aptamers combined with the photostability and small size of semiconductor nanocrystals offers a powerful and general tool for cellular imaging. This approach has particular promise in animal model systems to dynamically visualize and understand tumorigenesis at the cellular and molecular level and to screen and study targeted therapeutics. These studies also indicate that aptamer:nanocrystal conjugates may be suitable for in vivo labeling applications in patients. However, many additional hurdles must be overcome in order to reach this goal, including understanding toxicity and conjugate biodistribution, as well as potential limitations of in vivo imaging techniques themselves in terms of light penetration and optical detectability. If the toxicity of CdTe poses a problem for in vivo imaging, alternative nanocrystal chemistry, such as biocompatible passivation chemistry or an alternative material such as silicon perhaps, would be needed.

Acknowledgements

We thank Kristin Wall and Allison Nitsch for their help with LNCaP and PC3 cell cultures and Vivian Mack and Angela Bardo for their assistance with cell imaging. We also acknowledge partial financial support from the National Science Foundation, the Foundation for Research, the National Cancer Institute, the Robert A. Welch Foundation and the National Institutes of Health.

References

Barren III, R.J., Holmes, E.H., Boynton, A.L., Gregorakis, A., Elgamal, A.A., Cobb, O.E., Wilson, C.L., Ragde, H., Murphy, G.P., 1998. Prostate 36, 181–188.
Beigelman, L., McSwiggen, J.A., Draper, K.G., Gonzalez, C., Jensen, K., Karpeisky, A.M., Modak, A.S., Matulic-Adamic, J., DiRenzo, A.B., Haeberli, P., et al., 1995. J. Biol. Chem. 270, 25702–25708.
Bostwick, D.G., Pacelli, A., Blute, M., Roche, P., Murphy, G.P., 1998. Cancer 82, 2256–2261.
Chang, S.S., 2004. Drugs 5, 611–615.
Farokhzad, O.C., Jon, S., Khademhosseini, A, Tran, T.N., Lavan, D.A., Langer, R., 2004. Cancer Res. 64, 7668–7672.
Folkman, J., Moscona, A., 1978. Nature 273, 345–349.
Gao, X., Cui, Y., Levenson, R.M., Chung, L.W., Nie, S., 2004. Nat. Biotechnol. 22, 969–976.
Gaponik, N., Talapin, D.V., Rogach, A.L., Hoppe, K., Shevchenko, E.V., Kornowski, A., Eychmuller, A., Weller, H., 2002. J. Phys. Chem. B 106, 7177–7185.
Gospodarowicz, D., Greenburg, G., Birdwell, C.R., 1978. Cancer Res. 38, 4155–4171.
Greenlee, R.T., Hill-Harmon, M.B., Murray, T., Thun, M., 2001. Cancer statistics, 2001. CA Cancer J. Clin. 51, 15–36.
Gruber, H.E., Hanley Jr., E.N., 2000. BMC Musculoskelet. Disord. 1, 1.
Hoffman, R.M., 1991. Cancer Cells 3, 86–92.
Ingber, D.E., Dike, L., Hansen, L., Karp, S., Liley, H., Maniotis, A., McNamee, H., Mooney, D., Plopper, G., Sims, J., et al., 1994. Int. Rev. Cytol. 150, 173–224.
Jayasena, S.D., 1999. Clin. Chem. 45, 1628–1650.
Jenison, R.D., Gill, S.C., Pardi, A., Polisky, B., 1994. Science 263, 1425–1429.
Kawakami, M., Nakayama, J., 1997. Cancer Res. 57, 2321–2324.
Lato, S.M., Boles, A.R., Ellington, A.D., 1995. Chem. Biol. 2, 291–303.
Lim, Y.T., Kim, S., Nakayama, A., Stott, N.E., Bawendi, M.G., Frangioni, J.V., 2003. Mol. Imaging 2, 50–64.
Liu, C., Huang, H., Donate, F., Dickinson, C., Santucci, R., El-Sheikh, A., Vessella, R., Edgington, T.S., 2002. Cancer Res. 62, 5470–5475.
Liu, H., Moy, P., Kim, S., Xia, Y., Rajasekaran, A., Navarro, V., Knudsen, B., Bander, N.H., 1997. Cancer Res. 57, 3629–3634.
Lupold, S.E., Hicke, B.J., Lin, Y., Coffey, D.S., 2002. Cancer Res. 62, 4029–4033.
Michalet, X., Pinaud, F.F., Bentolila, L.A., Tsay, J.M., Doose, S., Li, J.J., Sundaresan, G., Wu, A.M., Gambhir, S.S., Weiss, S., 2005. Science 307, 538–544.
Miller, F.R., McEachern, D., Miller, B.E., 1989. Cancer Res. 49, 6091–6097.
Nelson, P.S., 2002. Ann. N.Y. Acad. Sci. 975, 232–246.
Peng, Z.A., Peng, X., 2001. J. Am. Chem. Soc. 123, 183–184.
Postma, R., Schroder, F.H., 2005. Eur. J. Cancer 41, 825–833.
Qin, P.Z., Pyle, A.M., 1999. Methods 18, 60–70.
Schaper, W., Ito, W.D., 1996. Circ. Res. 79, 911–919.
Slovin, S.F., 2005. Expert. Opin. Ther. Targets 9, 561–570.
Song, J., Rolfe, B.E., Hayward, I.P., Campbell, G.R., Campbell, J.H., 2000. In Vitro Cell Dev. Biol. Anim. 36, 600–610.
Tricoli, J.V., Schoenfeldt, M., Conley, B.A., 2004. Clin. Cancer Res. 10, 3943–3953.
Untergasser, G., Madersbacher, S., Berger, P., 2005. Exp. Gerontol. 40, 121–128.
Wuister, S.F., Swart, I., van Driel, F., Hickey, S.G., Donega, C.d.M., 2003. Nano Lett. 3, 503–507.
Yang, J., Richards, J., Bowman, P., Guzman, R., Enami, J., McCormick, K., Hamamoto, S., Pitelka, D., Nandi, S., 1979. Proc. Natl. Acad. Sci. U.S.A. 76, 3401–3405.